DOI: 10.17344/acsi.2019.5130 *Acta Chim. Slov.* **2019,** *66,* 686–693

Scientific paper

Micro and Nanostructure Surface and Interface Characterization of Anodized Zr in Two Different Electrolytes

Andrei Bogdan Stoian,[1] Maria Vardaki[1] and Ioana Demetrescu[1,2]*

[1] *Faculty of Applied Chemistry and Materials Science, Department of General Chemistry, University Politehnica of Bucharest, 1-7 Gheorghe Polizu str., 011061, Bucharest, Romania*

[2] *Academy of Romanian Scientists, 54 Spaiul Independentei, 050094, Bucharest, Romania*

** Corresponding author: E-mail: ioana_demetrescu@yahoo.com; i_demetrescu@chim.upb.ro Tel. +4 021 402 3930*

Received: 03-13-2019

Abstract

The present work reports on the morphologies and properties of anodized Zr in two different electrolytes. The Zr phosphates (α-ZP) obtained in the inorganic electrolyte containing H_3PO_4+NaF and zirconia (ZrO_2) nanostructures formed in the organic glycerol-based electrolyte were investigated by SEM, FT-IR and AFM. The surface analysis was completed by contact angles measurements. It was found that the type of electrolyte along with the applied voltage influence the structure of the sample and being more precise, the anodic oxidation in H_3PO_4 electrolyte promotes the evolution of flaky structures and eventually of pores by increasing the applied voltage, while the anodizing performed in glycerol-based electrolyte results in the formation of nanoporous structures that evolve into nanotubes as the applied voltage grows. Based on experimental data a film forming mechanism for α-ZP and ZrO_2 was proposed and correlated to analyzed surface properties.

Keywords: Zirconium phosphate; zirconia; anodizing; organic; inorganic; electrolyte

1. Introduction

Due to its remarkable physical, chemical and mechanical properties, zirconium (Zr) has been used in various fields including nuclear industry for having low neutron absorption and microelectronic industry for having high dielectric constant.[1,2] Zr is a strong, reactive valve metal that possesses physical and chemical properties similar to titanium (Ti) forming spontaneously a protective oxide film when it comes in contact with air. With a passive film, Zr presents an excellent resistance to corrosion in a variety of conditions, such as organic solutions, alkalis and acids and can be considered a promising and useful material that can be used in applications such as oxygen sensors,[3] protective coating materials in optical devices,[4] photocatalysts in environmental applications [5]and catalysts for fuel cells.[6] It is to mention that Zr is considered one of the most biocompatible elementsand a good choice for restorative works in oral cavity,[7–9] being a competition for Ti and Ti alloys.[10,11] Oral cavity environments are very aggressive not only because of saliva, but for their varying pH content as well, and the excellent resistance to corrosion of Zr and Zr alloys especially in combination with Ti is a strong point for recommendation as biomaterial.[12–14] The present work reports on formation of zirconium phosphates (α-ZP) as a result of anodizing in inorganic H_3PO_4+NaF electrolyte. It is important to know that α-ZP materials[15] thanks to their properties (thermal stability, ion exchange capability, good biological compatibility etc.) can be considered good candidates for a variety of applications, like for example to be used in catalysis[16] and photochemistry.[17] The ease of formation and modification along with the excellent properties makes α-ZP an urgent topic of ongoing research aiming to the extension of their applications in various fields,[18,19] being considered an old material with a bright future. Regarding the anodizing of Zr in the organic electrolyte, ZrO_2 nanostructures formed present desired qualities that proved to be useful for many applications, including biomedical field.[20] Further, it was found

that the way of self-organization of obtained ZrO_2 nanotubes appears to be very much alike to that proposed for Ti.[21,22] Zr anodic oxidation *via* electrochemical anodizing is a facile and inexpensive method for surface modification, providing the opportunity for obtaining a variety of different nanostructures based on the applied conditions (electrolyte, pH, applied voltage, post treatments etc.). In the present work is reported the fabrication of α-ZP and ZrO_2 nanostructures and shows how the used electrolyte and the applied electrochemical conditions during the anodizing process can affect the final structure, morphology and properties of the samples. Based on experimental data, a film forming mechanism for α-ZP and ZrO_2 was proposed and, as novelty, was direct correlated to analyzed surface properties.

2. Experimental

Zr samples (foil, thickness 0.1 mm, 99.98% – Sigma-Aldrich) were cleaned in an ultrasonic bath in distilled water and ethanol for 10 minutes each. The samples were then dried in atmosphere at room temperature. The surface modification was achieved by anodizing the samples with a Matrix MPS-7163 DC power supply. The anodizing was carried out for 60 minutes applying different voltages for each sample (5 V, 15 V, 45 V and 75 V) using the Zr sample as the anode and Pt foil as the cathode. Two sets of samples were produced by using different electrolytes. The first electrolyte (E1) containing 2M H_3PO_4 (85 wt.% – Sigma-Aldrich) and 30 mM NaF (>98% – Sigma-Aldrich) was used to obtain Zr phosphates and the second electrolyte (E2) containing glycerol 15vol% H_2O + 0.2M NH_4F was used to obtain ZrO_2 nanostructures.[23] The micro surface morphologies of the Zr samples were investigated with a Quanta 650 scanning electron microscope (SEM) from FEI in high vacuum at 10 kV. The coating thickness was evaluated by scratching the film and measuring the cross section with the SEM. The infrared spectra (FT-IR) were obtained with a Perkin-Elmer Spectrum 100 spectrometer in the range 4000–600 cm^{-1}. Micro roughness and adhesion forces were evaluated using an A.P.E. Research A100-SGS atomic force microscope (AFM) from 5 measurements for each sample. The wettability of the samples was evaluated with a CAM100 equipment from KSV Instruments using ultra-pure water. The contact angle values represent the average of 5 measurements.

3. Results and Discussion

3. 1. Surface Morphology

Fig. 1a shows the surface of Zr samples anodized in E1 at 5 V that are covered in two types of structures: the first type is represented by small semi-spheres with diameters of approximately 300 nm which form small clusters; the second type is represented by ridges with lengths of 1–3 μm and widths of 30 to 400 nm. On the same sample there was observed a phenomenon of bubble formation (10–100 μm diameter) and breaking, with the result of superficial stratum exfoliation. Outside the sites of former bubbles, a higher concentration of α-ZP ridges was observed. This observed process of bubble forming and braking was not completed during the anodizing time and on the surface are present sites in all development stages. Anodizing in E2 at the same voltage (Fig. 1b) led to the formation on the surface of the samples of an oxide layer with the thickness ranging between 200–400 nm. The oxide formation is the result of following reactions presented below[7]:

$$Zr + 2H_2O \rightarrow ZrO_2 + 4H^+ + 4e^-$$
$$ZrO_2 + 4H^+ + 6F^- \rightarrow [ZrF_6]^{2-} + 2H_2O$$

The role of fluoride ions in the oxide formation and in its stability has been reported in literature. ZrO_2 nanostructures formation in F^- containing electrolytes is the result of the competition between the electrochemical oxide formation and the chemical dissolution of said oxide

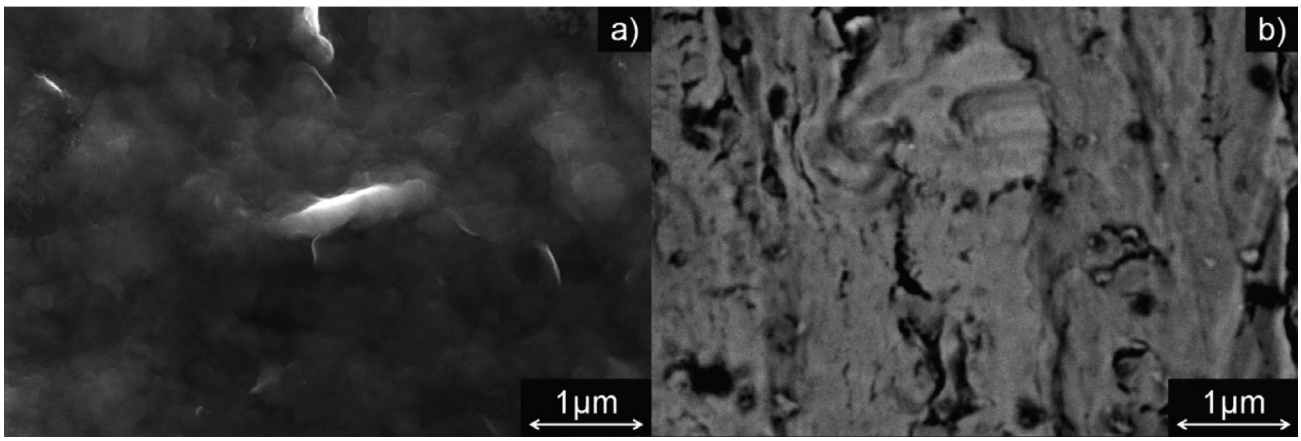

Fig. 1 SEM micrographies for Zr samples anodized at 5 V in a) E1; b) E2

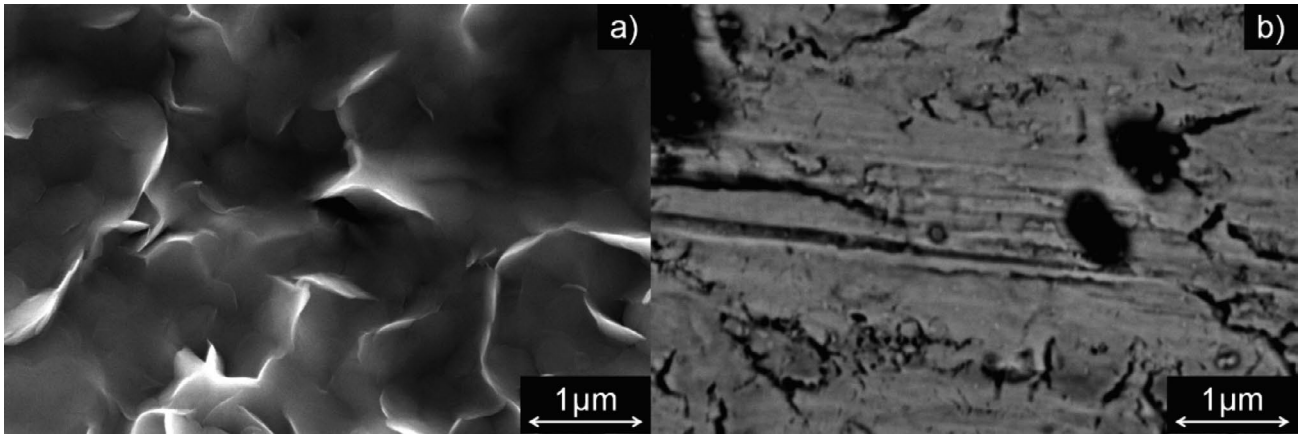

Fig. 2 SEM micrographies for Zr samples anodized at 15 V in a) E1; b) E2

through an intermediate stage where complex hexafluorozirconate anions form.

This oxide layer is covered in random cracks and incipient pores with diameters of around 100 nm start to appear.

At 15 V, anodizing in E1 led to a seemingly homogeneous surface shown in Fig. 2a. The two types of structures: semi-spheres (250 nm diameter) and ridges (length 300–800 nm and 60–100 nm width) are still present. However, in this case, the higher voltage led to an increased process speed. As such, there are no remaining bubbles on the surface at the end of the anodizing process, although the sites are still observable. The bubbles, which formed on the surface, were smaller (around 10 μm diameter) but denser. It is also evident that there are more α-ZP structures formed and at this voltage, they begin to take their classical flaked, laminar and aggregated shapes. Electrolyte E2 produced at 15 V a surface similar to the one obtained at 5 V (Fig. 2b). The differences occur in the dimensions of the surface features. The oxide layer is similar in thickness,

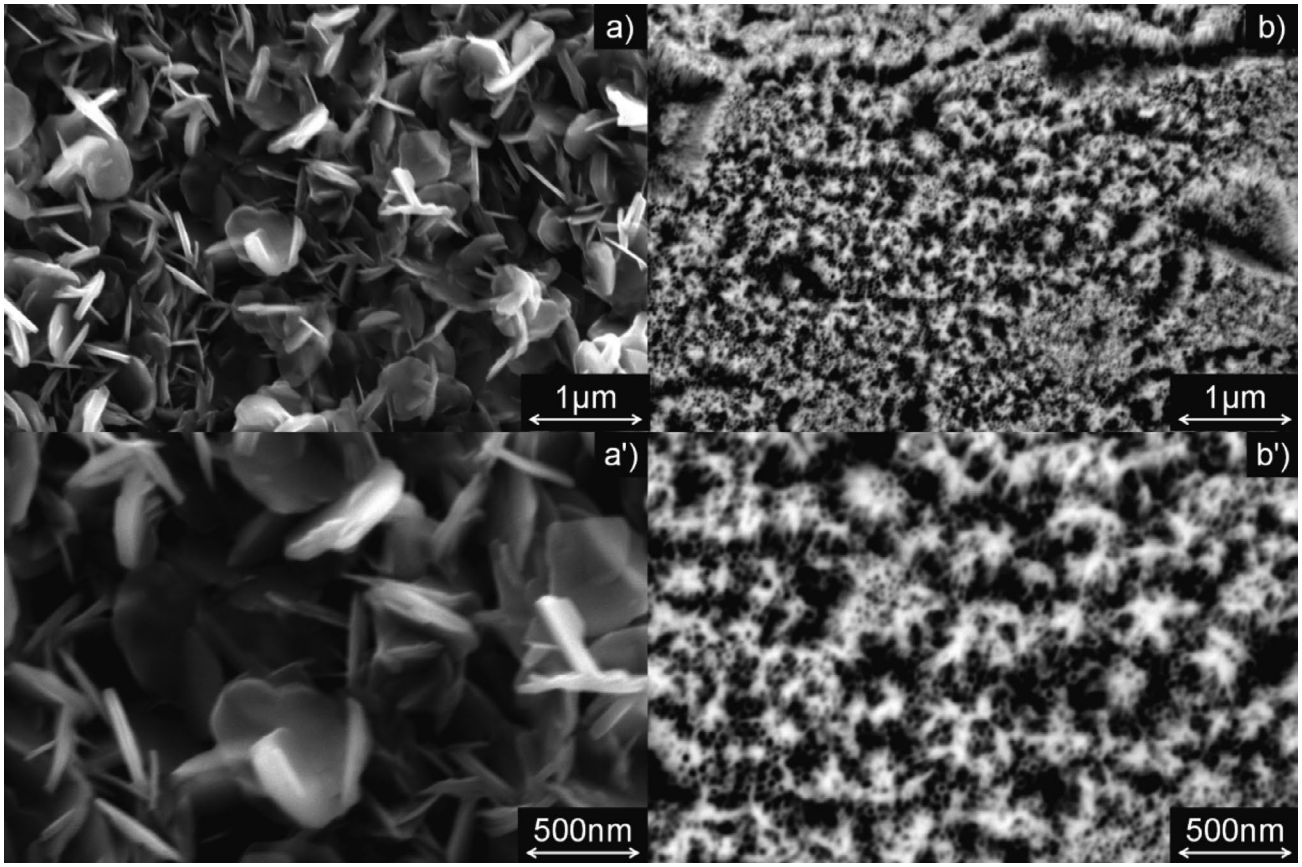

Fig. 3 SEM micrographies for Zr samples anodized at 45 V in a), a') E1; b), b') E2

but the cracks are deeper, wider, more numerous and the now well-formed pores have diameters between 100 nm and 4 μm.

When the anodizing voltage was increased to 45 V the sample anodized in E1 was completely covered with α-ZP structures (Fig. 3 a, a').

These quasi-hexagonal pellet structures had lengths of around 600 nm and thicknesses of around 80 nm and were not ordered in any particular direction. Underneath this stratum, a porous ZrO_2 surface was found present, with uniform pores having diameters of around 200 nm. Anodizing in E2 led to the covering of the Zr sample with ZrO_2 a mixture of nanopores, nanotubes and nanograss (Fig. 3 b, b'). Nanopores were observed on the thick initial oxide layer that hadn't dissolved totally at this voltage. The nanograss was found at the remaining boundary between the nanopore and nanotube layers and is probably a by-product of partial dissolution of the top porous layer. The nanotubes diameters range between 20 and 50 nm and the wall thickness is around 10 nm. Their length varies and are not particularly well organized. The tops of some of the nanotubes are covered and merge to form the nanograss.

At the highest studied anodizing voltage of 75 V, on the surface of the sample fabricated in E1 there are visible both α-ZP structures and a ZrO_2 surface covered with pores (Fig. 4a, a').

The α-ZP structures are found in laminated aggregates formed by multiple pellets and have sizes from 0.17 to 1 μm in length and 24 to 123 nm in thickness. The ZrO_2 pores present on the surface have diameters of around 400 nm. Anodizing in E2 led to the formation of two surfaces covered in nanotubes (Fig. 4b, b'). The first surfaces is represented by the initial oxide layer that partially dissolved which is now covered with closely packed nanotubes with diameters around 28 nm and wall thicknesses around 10 nm. The second surface positioned just beneath the first is represented by new oxide formed and dissolved during the anodization process at equilibrium. This surface is covered with larger and better organized nanotubes with diameters of around 75 nm and wall thicknesses around 14 nm.

3. 2. FT-IR Analysis

The corresponding FT-IR spectra of the obtained samples are shown in Fig.5. For the sample anodized in E1, the spectra[23] exhibit the characteristics vibration bands from the phosphate group (Fig. 5a). The broad band around 3150 cm^{-1} attributed to OH stretching of water molecules and the weak peak at around 1620 cm^{-1} indicates the bending of the water molecules. More water seems to be present on samples obtained at lower voltages. The strong band centered around 960 cm^{-1} corresponds to

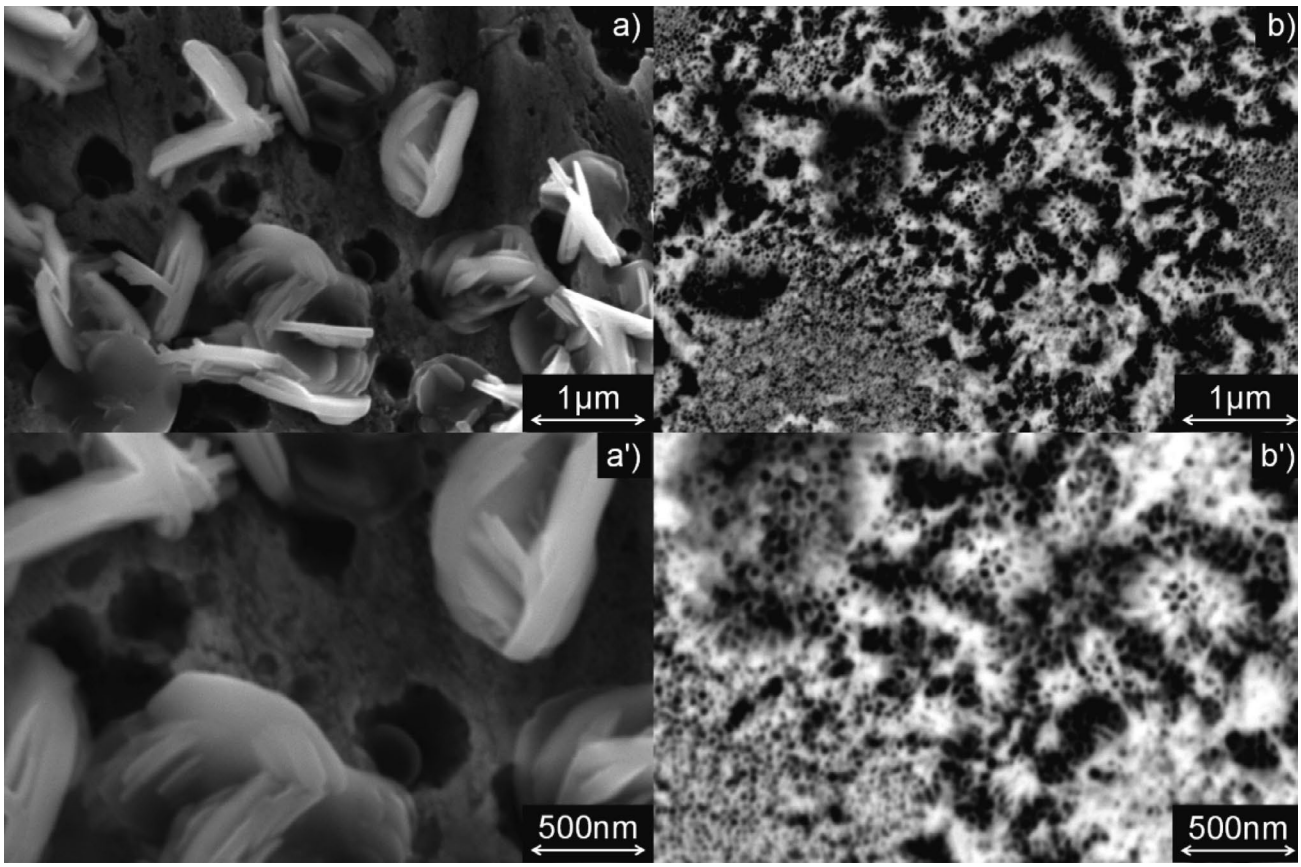

Fig.4 SEM micrographies for Zr samples anodized at 75 V in a), a') E1; b), b') E2

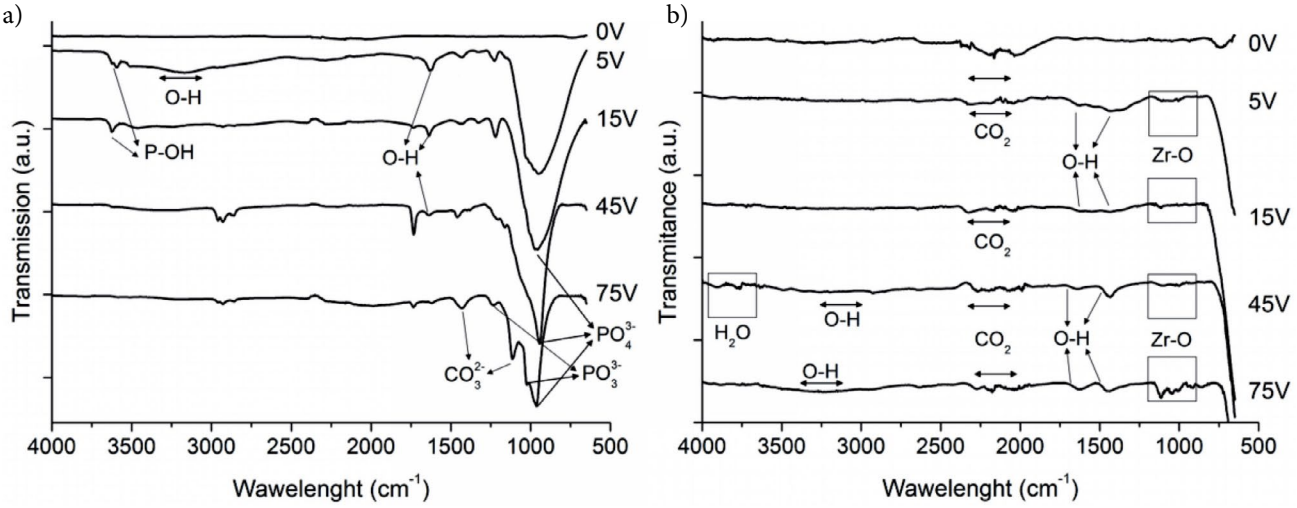

Fig. 5 FT-IR spectra for Zr samples covered with a) phosphates; b) oxides

some distorted tetrahedral phosphate groups in the nuclei of zirconium phosphates. The band at 1126 cm^{-1} corresponds to the deformation vibrations of P-O bonding of the PO_3 terminal groups. This band is only visible at the sample obtained at 75 V. Two bands at 3660 and 3643 cm^{-1} are due to free and hydrogen bonded surface P–OH groups respectively and are more evident for samples obtained at 5V and 15V. In the region of phosphate vibrations spectra of all samples exhibits bands at 1445, 1425, 1369, 1350 and 1208 cm^{-1}. These bands were observed in the FT-IR spectra of α-ZP. The two weak, bands at 1445 and 1425 cm^{-1} may be due to impurities of surface carbonate. The peaks attributed to phosphates become more well defined with the increase of the elaboration voltage.

The spectra anodized in E2 (Fig. 5b) show characteristic bands for ZrO_2 covered surfaces. The band around 3900–3600 cm^{-1} is characteristic for H_2O. The broad band around 3150 cm^{-1} attributed to OH stretching of water molecules and the weak peak at around 1620 cm^{-1} that indicates the bending of the water molecules is present on ZrO_2 samples as well. At around 2400–2200 cm^{-1} all samples show residues of CO_2. The absorbtion peaks of Zr-O vibrational bond are present for all the samples and the signal was found to be increasing with the anodizing voltage.

3. 3. Contact Angle Measurements

Contact angle measurements (Table 1) show that polished Zr is slightly hydrophillic. Samples covered with α-ZP show a constant decrease of contact angle values with the increase of the anodizing voltage. ZrO_2 samples show an increase of contact angle values at 5 V, reaching the limit of hydrophobicity, however, as the anodizing voltage increases, the contact angle values rapidly drop, reaching a state of super hydrophillicity at 75 V.

Table 1 Average contact angle values for Zr samples.

Applied voltage (V)	Contact angle (°) α-ZP	ZrO_2
0	69.1 ± 3.4	69.1 ± 3.4
5	35.5 ± 2	91 ± 4.1
15	32.4 ± 1.8	27.3 ± 2.1
45	31.6 ± 1.4	16 ± 1.2
75	26.1 ± 1.2	8.7 ± 0.7

3. 4. AFM Analysis

The roughness values (Ra) for the samples obtained in the two electrolytes are shown in Table 2.

Table 2 Average roughness values for Zr samples.

Applied voltage (V)	Ra (nm) α-ZP	ZrO_2
0	36 ± 4	36 ± 4
5	358 ± 16.9	85 ± 5.5
15	178 ± 9.2	36 ± 2.6
45	127 ± 8.1	40 ± 3.1
75	154 ± 8.7	29 ± 1.9

As can be noticed, the values for the roughness of the samples covered with α-ZP structures are around 4 times higher than those obtained for the samples covered with ZrO_2 nanotubes. However, the trend is similar, both types of samples experiencing an increase of roughness at 5 V, followed by a steady decrease as the voltage rises. This phenomenon can be attributed to the balance between phosphate/oxide formation and dissolution on and from the

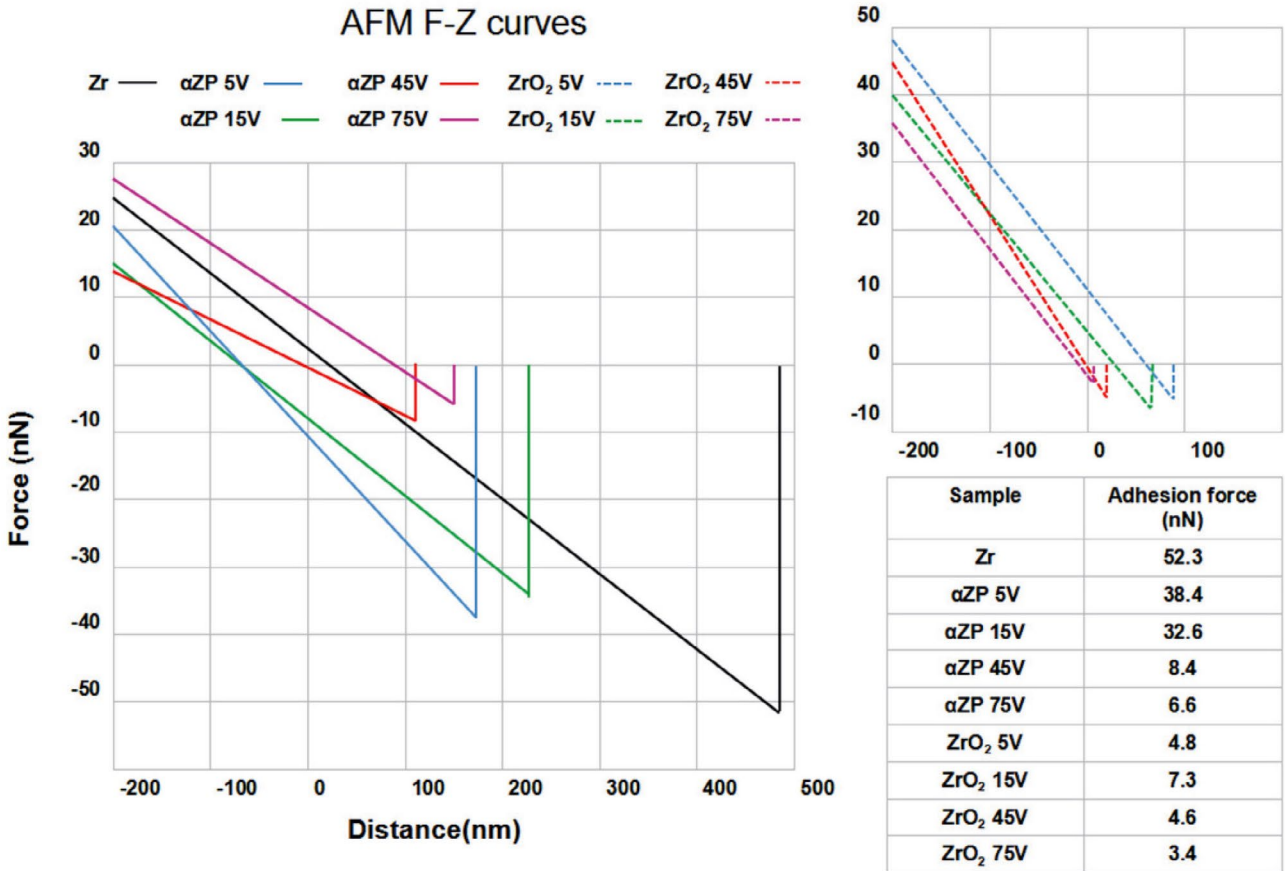

Sample	Adhesion force (nN)
Zr	52.3
αZP 5V	38.4
αZP 15V	32.6
αZP 45V	8.4
αZP 75V	6.6
ZrO_2 5V	4.8
ZrO_2 15V	7.3
ZrO_2 45V	4.6
ZrO_2 75V	3.4

Fig. 6 Normalized median values for AFM tip adhesion forces (F-Z curves)

samples surfaces during anodizing that is dependent on the applied voltage.

The normalized median values for the adhesion force measured with the AFM are shown as F-Z diagrams in Fig. 6. Polished Zr has the highest adhesion force, probably given by the smooth surface. This force is also active a great distance from the surface, the AFM tip being affected at around 480 nm from the surface. Samples covered with α-ZP structures have smaller attraction forces than bare Zr. The forces values and action range decrease steadily with the voltage.

The adhesion force measured by AFM experienced a decreasing trend with the increase of the sample elaboration voltage, suggesting the formed phosphate was the primary responsible for the reduction of the adhesion forces. Thin crystalline phosphates are produced on the Zr surface, the phosphate coating reducing the frictional force produced through shaping, drawing or slip processes ZrO_2 samples have the smallest forces that act only close to the surface. The capillaries on the surface provide better absorbent qualities, yielding different general surface qualities. The system formed by the SiC AFM tip and the surface of the samples experiences repulsive interactions mostly because of hydration forces which generate a decrease in friction coefficients and adhesion forces. The two surfaces seem to have different hardness levels, ZrO_2 surfaces producing higher displacements of the AFM tip than α-ZP surfaces at the maximum indentation depth.

Fig. 7 shows the probable film forming mechanism for α-ZP and ZrO_2 structures covered surfaces. From the gathered data, we deduced that competing phenomena are occurring on the surface during the anodizing process in both cases. These processes are: forming of Zr phosphates and/or oxides (depending on the electrolyte), dissolution of ZrF_6^{2-} complexes from the surface and forming of auto-organized zirconium compound structures. Regardless of the used electrolyte, these phenomena are influenced by the anodizing voltage which changes the balance and the speeds at which these phenomena occur, leading to different results. As was largely described in the literature,[22] anodizing parameters such as time, voltage, temperature and most important anodizing electrolyte composition are critical for the resulting desired morphologies. The composition of the sample surface seems to be less affected by the anodizing potential, instead being directly affected by the electrolyte composition.

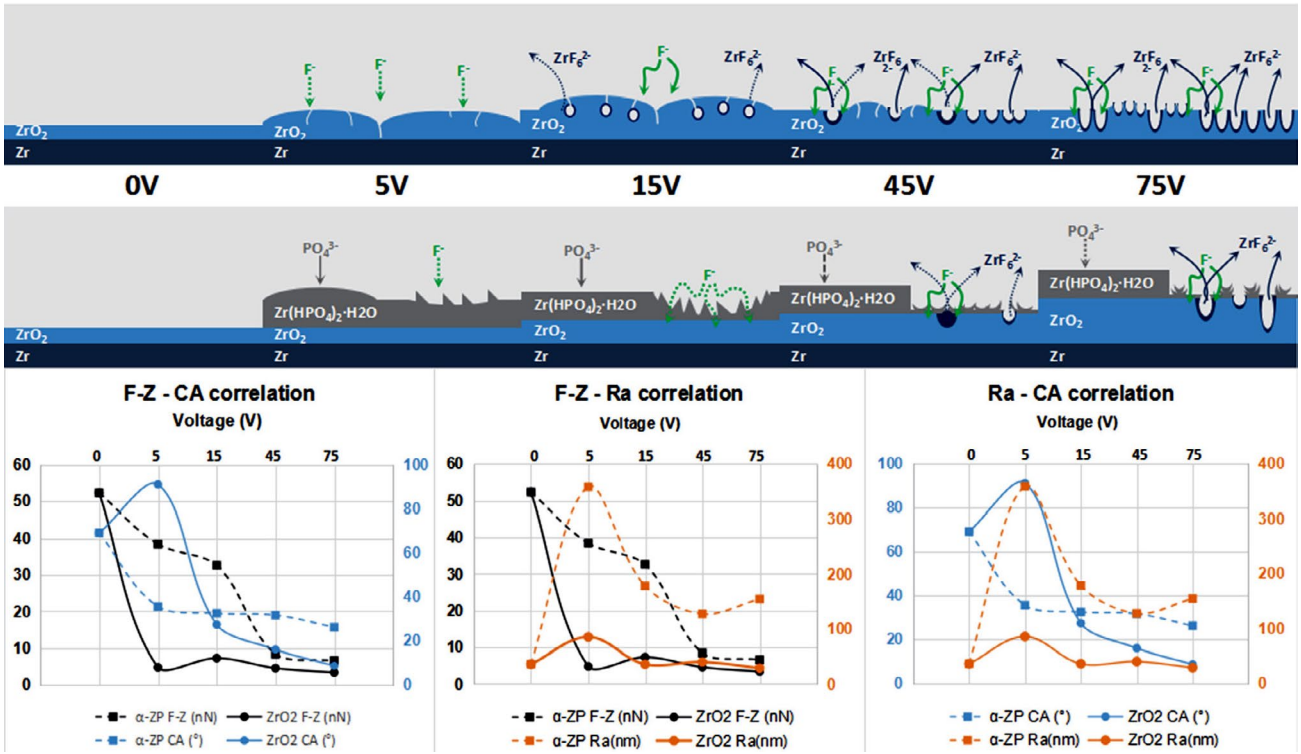

Fig. 7 Proposed film forming mechanism for α-ZP and ZrO_2 and correlation of analyzed surface properties

4. Conclusions

The SEM and AFM investigations revealed that structures with various sizes and shapes can be obtained by modifying the anodizing both the voltage and the electrolyte. On the surface of Zr anodized in H_3PO_4 α-ZP flake structures were obtained. These structures became more organized with the increase of the voltage and, at higher voltages, ZrO_2 pores began to form. When glycerol used, the formation of auto-organized nanotubes was found to be directly dependent on the applied voltage. The roughness is influenced by the type as well as by the degree of homogeneity of structures formed on the surfaces.The wettability and the AFM micro adhesion forces and roughness values can be correlated to some degree for both samples. In the case of orthopedic and dental implants it is usually reported that hydrophillic materials have higher biocompatibility, facilitating initial interaction between the biomaterial and the biofluids, thus promoting osseointegration. Roughness has a major role in the wettability of a biomaterial as well in the subsequent cell interaction with the implant surface. Based on all experimental data, a film forming mechanism for α-ZP and ZrO_2 was proposed and correlated to analyzed surface properties. From a physical concept, these results enable the understanding of the optimal properties needed for the development of damage-tolerant thin films leading to practical applications.

Acknowledgments

This work was supported by the Romanian Government National Council of Scientific Research in Higher Education (CNCSIS) – Executive Unit for Financing Higher Education, Research, Development and Innovation (UEFISCDI), project number PN-III-P4-ID PCE 2016-0316.

5. References

1. B. Cox, *J. Nucl. Mater.* **2005**, *336*, 331–368.
2. A. Gomez-Sanchez, M. Katunar, W. Schreiner, G. Duffó, S. Ceré, D. J. Schiffrin, *Acta Chim. Slov.* **2014**, *61*, 316–327. **DOI:**10.1016/j.jnucmat.2004.09.029
3. E. Ivers-Tiffee, K. H. Hardtl, W. Menesklou, J. Riegel, *Electrochim. Acta* **2001**, *47*, 807–814. **DOI:**10.1016/S0013-4686(01)00761-7
4. Q. Zhang, J. Shen, Wang, G. Wu, L. Chen, *Int. J. Inorg. Mater.* **2000**, *2*, 319–323. **DOI:**10.1016/S1466-6049(00)00037-4
5. A. I. Ahmed, S. A. El-Hakam, S. E. Samra, A. A. El-Khouly, A. S. Khder, *Colloids Surf. A Physicochem. Eng. Asp.* **2008**, *317*, 62–70. **DOI:**10.1016/j.colsurfa.2007.09.043
6. H. J. Cho, G. M. Choi, *J. Power Sources* **2008**, *176*, 96–101. **DOI:**10.1016/j.jpowsour.2007.09.118
7. D. E. Romonti, A. Gomez Sanchez, I. Milosev, I. Demetrescu, S. Cere, *Mater. Sci. Eng. C,* **2016**, *62*, 458–466.

DOI:10.1016/j.msec.2016.01.079
8. G. O. Buica, A. B. Stoian, D. Ionita, I. Demetrescu *Mater. Corros.* **2018**, *69*, 1713–1719. **DOI:**10.1002/maco.201810277
9. A. Gomez Sanchez, J. Ballarre, J. C. Orellano, G. Duffó, S. Cere, J. Mater. *Sci. Mater. Med.,* **2013**, *24*, 161–169. **DOI:**10.1007/s10856-012-4770-8
10. M.Mindroiu, E.Cicek, F. Miculescu, I. Demetrescu, *Rev. Chim. Bucharest* **2007**, *58*, 898–903.
11. I. Milošev, B. Kapun, V. S. Šelih, *Acta Chim. Slov*. **2013**, *60*, 543–555.
12. C. Vasilescu, S. I. Drob, P. Osiceanu, J. M. Calderon Moreno, M. Prodana, D. Ionita, I. Demetrescu, M. Marcu, I. A. Popovici, E. Vasilescu *Metall and Mat. Trans. A,* **2017**, *48*, 513–523. **DOI:**10.1007/s11661-016-3774-2
13. A. B. Stoian, M. Vardaki, D. Ionita, M. Enachescu, O. Brancoveanu, I. Demetrescu, *Ceram. Int.,* **2018**, *44*, 7026–7033. **DOI:**10.1016/j.ceramint.2018.01.137
14. S. Minagar, C. C. Berndt, J. Wang, E. Ivanowa, C. Wen, *Acta Biomater.* **2012**, *8*, 2875–2888. **DOI:**10.1016/j.actbio.2012.04.005
15. T. Hanawa, Y. Tsutsumi, Bioceram. Dev. Appl., **2010,** *1,* **DOI:**10.1007/s11661-016-3774-2
16. K. Segawa, S. Nakata, S. Asaoka, *Mater. Chem. Phys.* **1987**, *17*, 181–200. **DOI:**10.1016/0254-0584(87)90055-1
17. C. Kumar, A. Chaudhari, G. Rosenthal, *J. Am. Chem. Soc.* **1994**, *116*, 403–404. **DOI:**10.1021/ja00080a059
18. H. Xiao, S. Liu *Mater. Des.* **2018**, *155*, 19–35. **DOI:**10.1016/j.matdes.2018.05.041
19. M. Pica, A. Donnadio, M. Casciola, *Coord. Chem. Rev.* **2018**, *374*, 218–235. **DOI:**10.1016/j.ccr.2018.07.002
20. W. Jang, J. He, J. Zhong, J. Lu, S. Yuan, B. Liang, *Appl. Surf. Sci.,* **2014**, *307*, 407–413. **DOI:**10.1016/j.apsusc.2014.04.047
21. K. Yasuda, J. M. Macak, S. Berger, A. Ghicov, P. Schmuki, *J. Electrochem. Soc.* **2007**, *154*, C472–C478. **DOI:**10.1149/1.2749091
22. M. Kulkarni, A. Mazare, P. Schmuki, A. Iglic, *Adv. Mater. Lett.,* **2016**, *7*, 23–28. **DOI:**10.5185/amlett.2016.6156
23. F. Muratore, A. Baron-Wiechéc, T. Hashimoto, A. Gholinia, P. Skeldon, G. E. Thompson, *Electrochim. Acta,* **2011**, *56*, 10500–10506. **DOI:**10.1016/j.electacta.2010.12.089
24. X.g He, H. Xiao, H. Choi, A. Díaz, B. Mosby, A. Clearfield, H. Liang, *Colloids. Surf. A* **2014**, *452*, 32–38. **DOI:**10.1016/j.colsurfa.2014.03.041

Povzetek

Pričujoče delo obravnava morfologijo in lastnosti anodiziranega Zr v dveh različnih elektrolitih. Cirkonijev fosfat (α-ZP) smo pripravili v anorganskem elektrolitu, ki je vseboval H_3PO_4 in NaF. Nano cirkonijev oksid (ZrO_2) smo pripravili v elektrolitu na osnovi glicerola. Spojini smo karakterizirali z naslednjimi metodami vrstično elektronsko mikroskopijo (SEM), infrardečo spektroskopijo (FT-IR) in mikroskopom na atomsko silo (AFM). Analizo površine smo preiskovali tudi z meritvami kontaktnih kotov. Ugotovili smo, da vrsta elektrolita skupaj z uporabljeno napetostjo vpliva na strukturo vzorca. Anodna oksidacija v elektrolitu H_3PO_4 pospešuje nastanek in razvoj luskastih struktur in sčasoma por s povečanjem uporabljene napetosti. Pri procesu anodne oksidacije v elektrolitu na osnovi glicerola pa nastajajo nanoporozne strukture, ki se pri naraščanju napetosti razvijajo v nanocevke. Na podlagi eksperimentalnih podatkov smo predlagali mehanizma za oblikovanje α-ZP in ZrO_2 v povezavi z analiziranimi lastnostmi površin.